CYCLIC VOLTAMMETRIC AND EQCM STUDY OF THE BEHAVIOUR AND STABILITY OF PT-IR DEPOSITS AND PT-IR WIRE ELECTRODES FOR METHANOL ELECTROOXIDATION IN ACID SOLUTION

M.SOLEDAD URETA-ZAÑARTU, PATRICIA BRAVO, GLORIA REYES* AND CLAUDIA YAÑEZ

Departamento de Ciencias Químicas. Facultad de Química y Biología.
Universidad de Santiago de Chile. Casilla 40 correo 33 Santiago-Chile.

J.RAMON GANCELO, CLAUDIO GUTIERREZ AND JOSE F. MARCO

Instituto de Química-Física "Rocasolano", C.S.I.C., Spain

ABSTRACT

The electro-oxidation of methanol at Pt-Ir and Pt deposits, and at Pt, Ir, and Pt-Ir wires in sulfuric acid solution was studied by cyclic voltammetry (CV), and in the case of Pt-Ir and Pt electrodeposits, also with the electrochemical quartz crystal microbalance (EQCM). The effect of repetitive potential cycling on the Pt-Ir deposits, in the absence and presence of methanol, was also investigated by EQCM. Ir did not increase the activity of Pt for methanol oxidation, nor there was a significant effect of potential cycling on the activity of Pt-Ir electrodes. EQCM and CV results showed that potential cycling produced a sintering of the Pt-Ir codeposits without loss of Ir to the solution.

XPS analyses of cycled Pt-Ir/Ti electrodes showed that in the absence of methanol the Ir/Pt ratio decreased with cycling to one half of its value for the fresh deposit if the upper potential limit was 0.86 V *vs.* SCE, but increased by 30% if the said limit was increased to 1.1 V, showing the growth of an Ir oxide layer. Quite unexpectedly, cycling up to 1.1 V in the presence of methanol completely eliminated Pt(II) species from the surface, and decreased very much the fraction of Ir(IV) species.

KEY WORDS: methanol electrooxidation, bimetallic electrodes, EQCM, electrocatalysis

RESUMEN

En el presente trabajo se estudia la oxidación de metanol sobre electrodos preparados con aleaciones comerciales y depósitos de Pt-Ir así como de sus elementos puros utilizando la voltametría cíclica (CV) y la Electrobalanza de Cristal de Cuarzo (EQCM). El efecto del ciclado continuo de potencial en los depósitos de Pt-Ir, en ausencia y presencia de metanol, también fue investigado por EQCM. Los resultados indican el no aumento de la actividad de Pt para la oxidación de metanol en la aleación con Ir, así como tampoco se detectó un efecto significativo del ciclado de potencial en el electrodo. Tanto la técnica de EQCM como la de CV mostraron una sinterización del depósito de Pt-Ir sin pérdida de Ir a la solución.

Los resultados de XPS señalan que para electrodos de Pt-Ir/Ti ciclados en ausencia de metanol la razón Ir/Pt disminuye a la mitad respecto a su valor en un electrodo nuevo si el límite de potencial es de 0.86 V, pero aumenta en un 30% si este límite se aumenta a 1,1 V, evidenciando la formación de un óxido de iridio. Fuera de lo esperado, el ciclado del electrodo hasta 1,1 V en presencia de metanol, se elimina completamente la presencia de Pt(II) en la superficie electródica y disminuye en forma notoria la fracción de Ir que se encuentra como Ir(IV).

PALABRAS CLAVES: electro oxidación de metanol; electrodos bimetálicos, EQCM; electrocatálisis.

INTRODUCTION

In order to achieve a commercially viable Direct Methanol Fuel Cell much effort has been devoted to elucidate the mechanism of methanol electrooxidation on Pt [1,2]. A dual-path mechanism in which one path involves an active intermediate and the other one a poison intermediate, proposed for formic acid oxidation on platinum [3, 4], is also accepted for methanol [5]. The rate-limiting step is taken to be the chemical reaction between a methanol residue, typically chemisorbed CO, and a metal surface hydroxy species or activated water group [6], as follows:

$$Pt\text{-}CO + Pt\text{-}OH \rightarrow 2\ Pt + CO_2 + H^+ + e^- \qquad (1)$$

this requiring an overpotential of several hundred millivolts, due to the lack of oxygenated Pt species in the potential region, 0.0 - 0.6V vs. RHE, where methanol is adsorbed.

The nature of the adsorbate produced in the dissociative chemisorption of methanol on Pt has been studied using in situ IR spectroscopy at polycrystalline [7,8] and single crystal Pt electrodes [5], Electrochemical Quartz Crystal Microbalance (EQCM) [9,10], and Differential Electrochemical Mass Spectrometry (DEMS) [11].

The activity of Ir for methanol electrooxidation is very low [12, 13]. CO linearly chemisorbed on Ir, as well as dissolved CO_2 and formate, have been identified by FTIR spectroscopy in the electrooxidation of 1M methanol on Ir in acidic media [13]. However, hydrated iridium oxide has been proposed as a good catalyst for methanol electro-oxidation, since (i) electrooxidation of Ir begins at lower potentials than that of Pt (ii) hydrated iridium oxide is stable with respect to temperature and pH changes within the ranges in which direct methanol fuel cells work and (iii) its preparation from iridium as well as its reactivation are straightforward [14].

Increased rates of methanol oxidation, as compared with pure Pt, have been obtained by alloying Pt with other noble metal, e.g. Pt/Ru [15,16,17] and Pt/Au on graphite [18]. Various mechanisms have been proposed to explain this enhancement: (i) modification of the electronic properties of Pt, (ii) the bifunctional mechanism of catalysis and (iii) the "third body" or blocking effect [19]. In the bifunctional mechanism the second metal (Ir) would facilitate the oxidation of a CO (or COH) intermediary strongly adsorbed on Pt by supplying oxygen atoms at an adjacent Ir surface site, since the formation of iridium oxygenated compounds in acidic medium starts at a potential about 0.3 V less positive than on Pt [20].

The objectives of this work were: (i) to prepare high surface area Pt-Ir electrodeposited electrodes and to evaluate their activity and stability upon potential cycling (ii) to compare electrodeposited Pt-Ir electrodes with a 70-30 Pt-Ir commercial alloy wire, and (iii) to evaluate the stability of the Pt-Ir deposits by repetitive potential cycling and EQCM..

EXPERIMENTAL SECTION

Electrode preparation

Pt-Ir films were obtained by electrodeposition at constant current density (10 mA cm^{-2}) as already described [20]. The substrates were either a Ti foil (99,7%, Aldrich) (Pt-Ir/Ti electrode) or a 10 MHz AT-cut quartz crystal (Elchema) with a thin gold film on both sides (Pt-Ir/Au/Q electrode). The mass of Pt-Ir in the Pt-Ir/Au/Q electrodes was close to 20 mg. The electrolytic bath contained hexachloroplatinic (IV) acid (about 10% acidic solution containing 3.8% Pt, Merck) and sodium hexachloroiridate (IV) trihydrate (99.9 %, Aldrich) in 0.5M H_2SO_4 (Merck p.a.) with a 70/30 Pt/Ir atomic ratio. Earlier work [21] with Pt-Ir/Ti electrodes showed a good correlation between the atomic ratios of the metal components in the plating bath and in the electrodeposit. Pt wire (Aldrich, 0.5 mm diam.), Ir wire (Aldrich, 0.5 mm diam.) and 70:30 Pt:Ir wire (Aldrich, 0.5 mm diam.) were also used.

Electrode characterization

The electrodes were tested by cyclic voltammetry (CV) in 0.5M H_2SO_4 deoxygenated solution, using a Wenking potentiostat. The roughness factor R_F (real area/geometric area) was calculated from the hydrogen desorption charge ($Q°_H$), assuming 220 and 224 mC cm^{-2} for a monolayer of adsorbed hydrogen on Ir and Pt, respectively [21]. A Pt helix of high area was used as counter electrode (CE), and the reference electrode (RE) was a saturated calomel electrode (SCE) connected a Luggin capillary situated close to the working electrode (WE). All potentials are referred to the SCE.

An Electrochemical Quartz Crystal Microbalance (EQCM-501-Elchema) with 10 MHz AT-cut quartz oscillators with a calibration constant of 4.4 ng Hz^{-1} cm^{-2} was used. An Elchema PS 205 potentiostat and a 16-bit data acquisition system with real-time data acquisition software, Voltscan 3.0, were used for simultaneous recording of CVs and frequency-potential curves. Both the mass and the current densities were always referred to the geometric area of the electrodes unless otherwise indicated.

The Pt-Ir deposits were subjected to repetitive potential cycling (RPC) at 0.1 V s^{-1} up to two potential limits, 0.86 V and 1.1 V, in 0.5M H_2SO_4 solutions with and without methanol. During the last cycle the mode of the Wenking potentiostat was changed from "periodic triangle" to "single triangle", so that after cycling the electrode remained at the initial potential. Cycled Pt-Ir/Ti electrodes were also characterized by *ex situ* X-Ray Photoelectron Spectroscopy (XPS). The XPS data were recorded at a take-off angle of 90° with a triple channeltron CLAM2 analyzer using Al Ka radiation and a constant analyzer transmission energy of 100 eV for the wide scan spectra, and 20 eV for the narrow scan spectra. Base pressure in the analyzer was typically in the 10^{-9} mbar range. All binding energy (BE) values were referred to the adventitious C 1s signal (284.6 eV).

The BE values are accurate to ±0.2 eV. All the spectra were computer fitted. Relative atomic concentrations were calculated using tabulated atomic sensitivity factors [22].

RESULTS AND DISCUSSION

Cyclic Voltammetry

The dashed curves in Figure 1 A-C are CVs at 0.1 Vs^{-1} of 70:30 Pt:Ir (A), Ir (B) and Pt (C) wire electrodes in 0.5M H_2SO_4. The current densities are referred to the geometric area, which allows to estimate if diffusion-limited electrooxidation of bulk solution species is achieved. The Pt and Pt-Ir wires show similar CVs, and different from that of Ir wire. This is more clearly seen in the plot of (anodic charge/ R_F) *vs.* E for the positive sweep of the CVs (Fig 1D), in which the curves 1 of Pt (solid line) and Pt/Ir (dashed line) wires almost overlap. As is well known, the CV of Ir on which an oxide layer has been grown by RPC between the hydrogen evolution region (HER) and the oxygen evolution region (OER) (dashed line in Figure 1B) shows no double layer region, and shows a prepeak at 0.4 V due to formation of surface oxides and the well-known reversible peak at 0.7 V attributed to a surface Ir(III)/Ir(IV) process [23]. Although formation of the surface oxide on Ir begins at a lower potential than on Pt, on the Pt-Ir wire oxide formation begins at the same potential as on Pt.

The solid lines in Figures 1 A-C are the second CVs after methanol introduction at open circuit under nitrogen stirring followed by 30 s of polarization at 0.23 V. For both Pt-Ir and Pt wires (solid lines in Figs.1 A and C, respectively) methanol lowers the hydrogen desorption/adsorption charge, since it chemisorbs dissociatively, yielding mostly chemisorbed CO [24]. A methanol oxidation peak at ca. 0.6 V, where metal oxidation starts, and also an anodic peak at about 0.45 V in the negative sweep, corresponding to methanol oxidation on the freshly reduced metal, are observed. On the contrary, Ir shows very little activity towards methanol oxidation, and only in the positive scan (Fig 1 B, solid line), since reduction of Ir surface oxide in the negative scan is not complete. Methanol oxidation on Ir wire is very dependent on scan rate, methanol concentration and positive potential limit, as observed by Aramata et al. [25]. Curves 3 in Fig. 1D show that oxidation of the methanol residue begins at almost the same potential for Pt/Ir (dashed line) and Pt (solid line) wires, and that the charge is slightly higher for Pt. Therefore, no improvement of methanol electrooxidation accrues from Ir alloying of Pt.

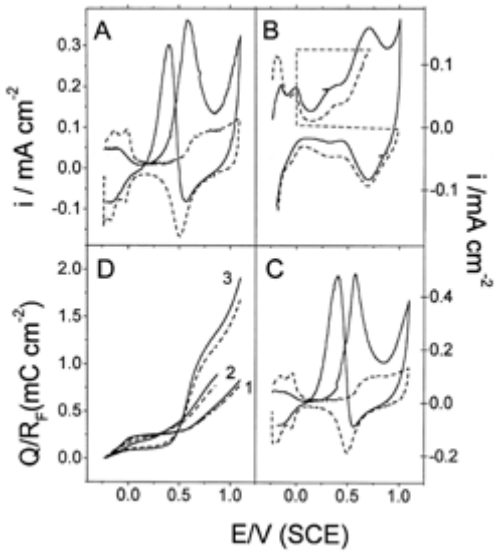

Fig. 1. Cyclic voltammograms at 0.1 Vs^{-1} in 0.5M H_2SO_4 without (dashed lines) and with 0.1 M CH_3OH (solid lines) for: A: 70/30 Pt-Ir wire (R_F=1.2) B: Ir wire (R_F=1.3); and C: Pt wire electrodes (R_F = 1.3) R_F: roughness factor. D: Q/R_F vs. E plot for (1) Pt wire (solid) and Pt-Ir wire (dashed) in the absence of methanol; (2) Ir wire in the presence (solid) and the absence (dashed) of methanol and (3) Pt wire (solid) and Pt-Ir wire (dashed) in the presence of methanol.

The values of *d*log(peak current density)/*d*log(scan rate) for methanol oxidation on the different electrodes (Table I) correspond neither to control by diffusion from the bulk nor to a surface process. In any case, it is obvious that methanol oxidation is not under diffusion control for any of the electrodes, since the peak current densities per unit geometric area (Figs. 1 A-C) are at least one order of magnitude smaller than the calculated one for diffusion-controlled irreversible oxidation of methanol.

Table I. CV parameters for methanol oxidation

		$d\log(I_p)$	dE_p
electrode	R_F	$d\log(\nu)$	$d\log(\nu)$
Ir wire	1.30	0.74±0.08	0.03 at low v 0.166 at high v
Pt wire	1.34	0.43±0.03	0.023±0.002
Pt-Ir wire	1.2	0.36±0.07	0.025±0.02
Pt-Ir / Ti	13.4	0.19±0.03	0.099±0.016
Pt/Ti	22.9	0.27±0.02	0.055±0.008
Pt-Ir/Au/Q	26.9		
Pt/Au/Q	11.9		

Much has been written about the influence of electrode roughness on electrocatalytic activity. According to Visscher et al. [26], a platinized platinum electrode (Pt/Pt) will behave as smooth Pt only if its roughness factor is less than 10.

Figure 2 shows the sixth CVs of Pt-Ir /Ti deposits (A) and Pt /Ti deposits (B) in 0.5 M H_2SO_4 in the absence (dashed line) and in the presence (solid line) of 0.1 M CH_3OH, and the corresponding Q/R_F vs. E plot (C) for the positive scan. The CVs are similar to those in Fig. 1 for Pt and Pt-Ir wires, although for the Pt-Ir deposit in methanol the oxidation current in the reverse scan is so high that the net current is always anodic. Contrary to the behaviour of wire electrodes, in the positive sweep the anodic charge with methanol is slightly higher for the Pt-Ir deposit than for the Pt deposit (solid and dashed lines, respectively, of curves 2 in Fig. 2C). Again, the presence of Ir does not shift negatively, *i.e.* does not catalyze, the start of methanol electrooxidation on Pt.

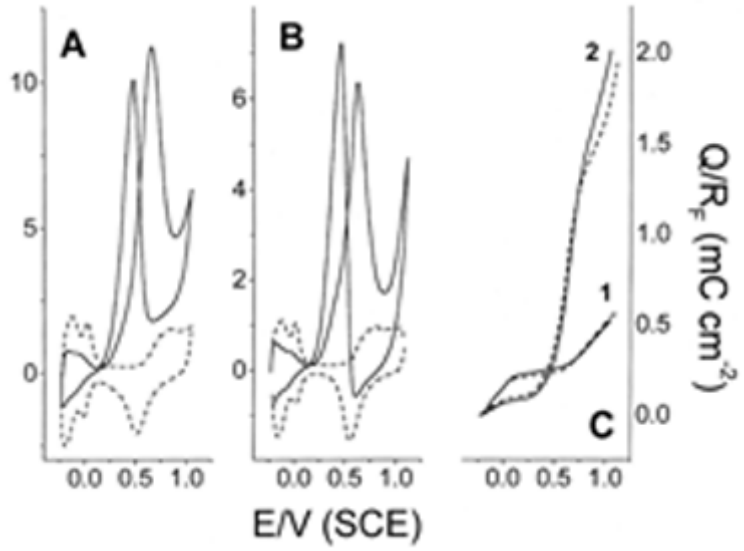

Fig. 2. Cyclic voltammograms at 0.1 V s^{-1} in 0.5 M H_2SO_4 without (dashed lines) and with 0.1 M CH_3OH (solid lines) for: A: Pt-Ir electrodeposited on Ti (R_F=22.8). B: Pt electrodeposited on Ti (R_F=13.3) ; C: Q/R_F vs. E plot for (1) Pt-Ir/Ti deposit (solid) and Pt/Ti deposit (dashed) in the absence of methanol; (2) Pt-Ir/Ti deposit (solid) and Pt/Ti deposit (dashed) in the presence of methanol.

EQCM measurements of electrodeposited Pt/Au/Q and Pt-Ir/Au/Q electrodes in the absence and presence of methanol

As the electrodeposited and wire electrodes have similar CVs, EQCM measurements on the former will be representative of the behaviour of the latter. Although the oxidation of methanol is a very complex reaction indeed, which makes difficult to separate the contributions of chemisorbed species, adsorbed anions, and adsorbed water molecules to the total mass change, the Dm/E curves can be qualitatively interpreted, especially in the potential region of adsorption and desorption of methanol adsorbates and intermediaries.

The sixth CVs and corresponding $\Delta m/E$ curves at 20 mV s^{-1} in 0.5M H_2SO_4 without (solid line) and with 1M CH_3OH (dashed line) are plotted in Figure 3 A-C for Pt/Au/Q (R_F=11.9) deposits, and in Figure 3 D-F for Pt-Ir/Au/Q (R_F=26.9) deposits. The mass changes are referred to the geometric area of the electrodes. For the Pt/Au/Q deposit in 0.5M H_2SO_4 (Figure 3 B and C, solid line) the results are similar to those in the literature [26, 27] and have been described in terms of adsorption and desorption of

water and/or anions and oxidation of the electrode surface [28, 29]. The Dm/E profile for the Pt/Au/Q deposit in the presence and the absence of methanol was essentially reproducible for many different electrodes.

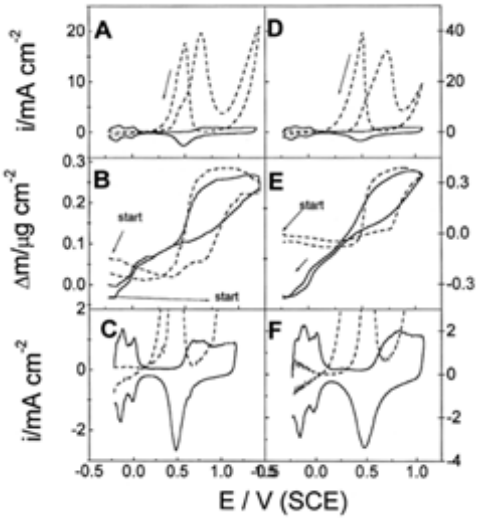

Fig.3. Cyclic voltammetric and mass response of a Pt/Au/Q deposit (AÆC) and of a Pt-Ir/Au/Q deposit (DÆF) in 0.5 M H_2SO_4 in the presence (dashed line) and absence (solid line) of 1M CH_3OH at 20 mVs^{-1}. In C and F the same CVs that appear in A and D are given again, but with a suitable current scale. Geometric area = 0.24 cm^2: Mass deposited: Pt, 7 mg, R_F = 11.9 Pt-Ir, 20 mg. R_F = 26.9

In Figure 3 B and E, Dm/E curves obtained in the presence (dashed line) and in the absence (solid line) of methanol have been superposed, assuming that the amount of oxide formed at the positive scan limit is not altered by methanol, as has been assumed for Pt/Au/Q deposits [26]. The initial mass is higher in the presence of methanol for both electrodes, unquestionably due to the presence of chemisorbed CO produced by the dissociative chemisorption of methanol at open circuit, which completely inhibits the adsorption of H on both Pt and Pt-Ir deposits, as can be seen in the CVs of Figs. 3C and 3F, respectively. The mass increase due to the adsorption of CO at the beginning of the sweep is 102 and 346 ng cm^{-2} for Pt and Pt-Ir, respectively, which are approximately proportional to the roughness factors of the two deposits, 11.9 and 26.9, respectively.

In the presence of methanol, in the double layer region the mass decreases slowly with increasing potential for the Pt deposit (dashed line in Figure 3 B), while for the Pt-Ir deposit it barely decreases. Between 0.45 and 0.75 V, the potential range of the anodic peak, the mass increases slightly for both electrodes, indicating the beginning of metal electrooxidation. Finally, at 0.75 V the mass increases steeply due to formation of an oxide monolayer.

In the negative sweep, for both deposits the mass decreases steeply at the potential at which methanol oxidation on the freshly reduced metal starts (dashed lines in Figs. 3 A and D, respectively), which is the same for both electrodes. It should be remarked that for both Pt and Pt-Ir deposits the potential of the peak of methanol oxidation in the reverse scan is about the same of the methanol oxidation shoulder, 0.45 V, in the positive sweep.

In Fig. 4 we show normalized current densities, j/R_F (Fig. 4 A), normalized anodic charges, Q/R_F (Fig. 4 B) and normalized mass changes, Dm/R_F (Fig. 4C) during a positive potential scan after five previous CVs, for both Pt and Pt-Ir (dashed and solid lines, respectively) in 0.5 M H_2SO_4. In Figure 4 D the plot of Dm/R_F vs. Q/R_F is given.

Normalization by R_F was carried out because the porosity of the deposit can seriously affect the results of EQCM, since the liquid trapped in the pores can give an extra mass contribution [26].

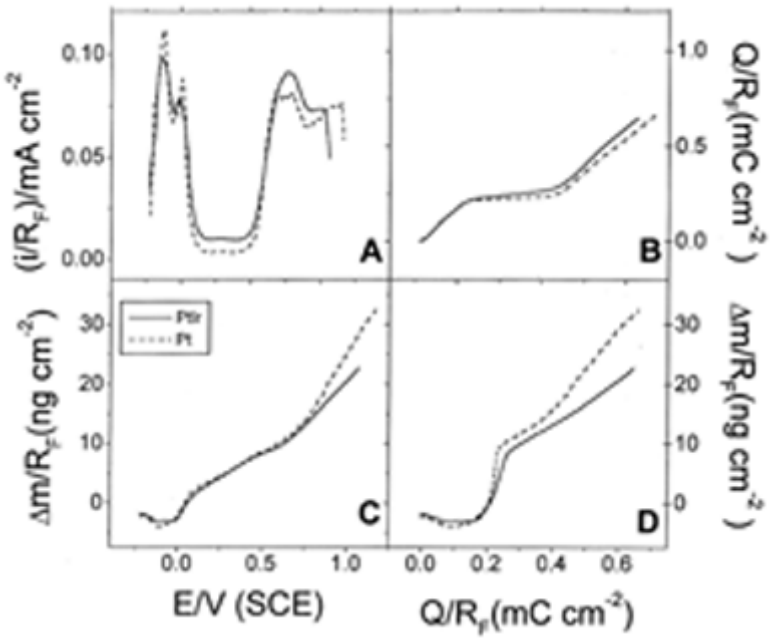

Fig.4. Normalized (by R_F) voltammetric and EQCM responses of a Pt-Ir/Au/Q deposit (solid line) and a Pt/Au/Q deposit (dashed line) during a positive potential sweep at 0.1 V s^{-1} in 0.5 M H_2SO_4 A: Current density i/R_F vs. E; B: charge, Q/R_F vs. E; C: mass change, Dm/R_F vs. E and D: Dm/R_F vs. Q/R_F.

Both in the Pt-Ir wire and in the Pt-Ir deposits the normalized current density in the double layer region is higher for Pt-Ir than for Pt (Fig. 4 A), since Ir oxidizes to some extent in this potential range. This is also apparent in the plot of the normalized charge (Fig. 4 B), and still more clearly in the Dm/R_F vs. Q/R_F plot (Fig. 4 D), where for Pt (dashed line) the nearly vertical section clearly corresponds to the double layer region, in which the mass increases due to water and/or anion adsorption with a negligible change in charge, while for Pt-Ir (solid line) there is a charge increase in the double layer region of DQ/R_F = 43mC cm^{-2} and consequently this section becomes less steep.

The normalized mass change is approximately the same for Pt and Pt-Ir deposits (dashed and solid lines in Fig. 3 C, respectively) up to 0.7 V, in agreement with the CVs in Fig. 3 A. At higher potentials the normalized mass increase is higher for Pt than for Pt-Ir, again in agreement with the higher normalized current density of the former in the CVs.

If the Pt-Ir deposit is subjected to a positive ramp at 0.1 V s^{-1} up to 1.1 V and then held at this potential for 100 s, the mass at the beginning of the 100 s period is the same in the absence or presence of methanol, and increases to a final mass about 45 ng cm^{-2} higher, also irrespective of the presence of methanol. This shows that, even if methanol electrooxidation proceeds by a chemical reaction between methanol and the metal oxide(s), this does not affect the amount of metal oxide formed, since the metal would be reoxidized immediately, as was to be expected.

Influence of potential cycling on Pt-Ir/Au/Q and Pt-Ir/Ti deposits in the absence and presence of methanol

Repetitive potential cycling of Pt-Ir deposits was carried out at 0.1 V s^{-1} up to two positive potential limits, 0.86 V and 1.1 V, in 0.5 M H_2SO_4 solutions with and without methanol. These two potentials were chosen because 0.86 V corresponds to the current minimum after the methanol oxidation peak, and 1.1 V to a high oxidation current in the presence of methanol.

Cycling in the absence of methanol

Cycling a Pt-Ir/Au/Q deposit in 0.5 M H_2SO_4 up to 0.86 V and 1.1 V increases the definition of the hydrogen peaks, although the current decreases (Figs. 5 A and B, respectively).

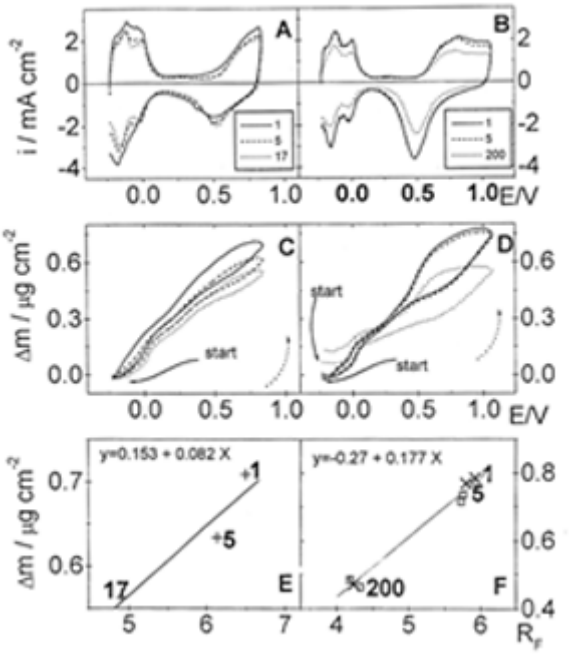

Fig. 5. Repetitive cyclic voltammograms at 0.1 V s^{-1} (A, B) and simultaneously recorded mass response (C, D) of Pt-Ir/Au/Q deposit in 0.5 M H_2SO_4. Two positive potential limits were used, 0.86 V (A and C; CVs 1, 5 and 17) and 1.1 V (B and D; CVs 1, 5 and 200). E and F , plots of the total mass change (difference between the masses at the positive and negative limits of the sweep) vs. R_F for a positive sweep of limit 0.86 V (E) and 1.1 V (F). The linearity of plots E and F shows that the decrease in mass change is due to a sintering of the deposits, not to metal dissolution.

The simultaneously recorded Dm/E curves are shown in Figs. 5 C and D without changes in offset. The plots of the total mass change vs. R_F as cycling proceeds are given in Figures 5 E and F for positive potential limits of 0.86 V and 1.1 V, respectively**.**

Cycling up to 0.86 V decreases the total mass change by 20%, but not the initial mass (Fig. 5 C). The mass decrease is approximately proportional to the decrease in real surface (Fig. 5 E), since R_F also decreases by 25%, from 6.5 to 4.9. Therefore, it is clear that the mass decrease is due to a sinterization of the deposit, rather than to dissolution.

Cycling up to 1.1 V also decreases initially the mass in the oxide zone, but after several cycles the mass begins to increase in the hydrogen region. This mass increase is not due to the presence of Ir, since it was also observed with Pt deposits (not shown).

The decrease of the total mass change after 200 scans up to 1.1 V (Figure 5 D) was 35%, which is similar to the decrease in R_F of 29%, from 5.9 to 4.2, this indicating again that the decrease in mass is due to sintering of the deposit. The plot of the total mass change *vs.* R_F (Fig. 5 F) shows excellent agreement between the results corresponding to the data in Figs. 5 B and D (crosses) and those corresponding to another experiment (squares), showing again an approximately linear relationship between the total mass change and R_F, as was to be expected.

Cycling in the presence of methanol

With both Pt-Ir/Ti and Pt-Ir/Au/Q deposits, in repetitive CVs at 0.1 V s^{-1} in 0.5 M H_2SO_4, + 1 M CH_3OH (recorded after one characterization CV in 0.5M H_2SO_4 base electrolyte) both peaks of methanol oxidation increased initially with cycling up to 0.86 V (not shown) and 1.1 V and then decreased slowly. We will discuss only the results obtained with the higher positive limit, since those obtained with the lower one were very similar.

Figure 6 A shows the 1st, 5th and 200th CV up to 1.1 V in the presence of methanol for a Pt-Ir/Au/Q deposit (R_F=6.1). In Figure 6 B we have superposed the mass responses in the hydrogen and double layer region. (It should be stressed that it is difficult to set the mass to zero at the initial scan potential, due to the very high sensivity of the EQCM, so that in order to effect a comparison the curves should be shifted vertically until they coincide in a chosen region). Poisoning of the Pt-Ir surface by chemisorbed CO inhibits the adsorption of water/anions, and consequently the total mass increases are lower than those in the absence of methanol for a Pt-Ir deposit with a similar R_F, 5.9 (Fig. 5 D).

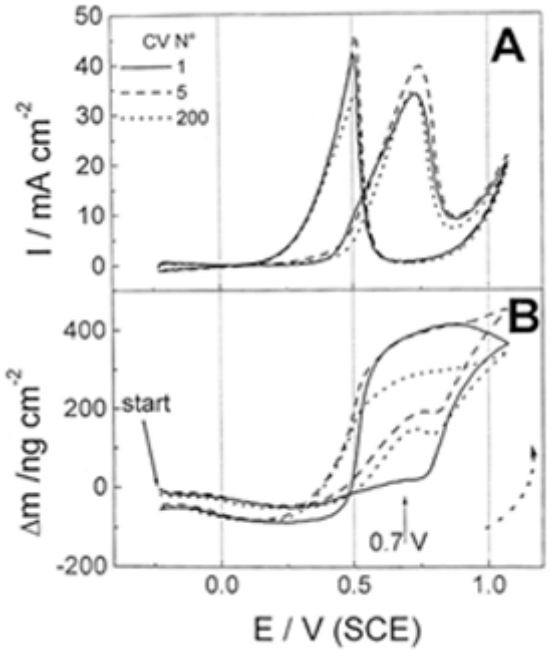

Fig.6. Repetitive cyclic voltammograms at 0.1 Vs^{-1} up to 1.1V (A) and simultaneously recorded mass response of Pt-Ir/Au/Q in 0.5M H_2SO_4 + 1M CH_3OH (B). The voltammogram number is indicated in Fig. 6 A.

A very interesting fact is that in the positive sweep of the fifth CV the mass starts to increase at a potential 0.25 V less positive than in the first CV (Fig. 6 B), while in the absence of methanol the fifth and first sweep practically coincided (Fig. 5 D). This negative shift with cycling of the start of the mass increase could be attributed to a decrease with cycling of poisoning by methanol residues, a hypothesis which is supported by the fact that the peak of methanol oxidation starts at a 0.2 V lower potential, and its peak current density is 17% higher, in the fifth than in the first positive sweep (Fig. 6 A), possibly due to a change in the structure of the oxide (see below).

In any case, the power of EQCM to detect differences in electrochemical behaviour that are not readily apparent in the CVs is clearly evidenced. In the negative scan the two Dm/E curves overlap initially, after which the mass decreases less rapidly in the fifth than in the first CV, although eventually the mass in the hydrogen zone is the same.

XPS analysis of Pt-Ir/Ti electrodes previously cycled in the absence and presence of methanol

In order to determine the influence of methanol on Pt-Ir deposits their XPS spectra were obtained *ex situ* after cycling in the absence and presence of methanol. As is well known, *ex situ* measurements may not reflect the state of the electrode in the electrochemical cell, although the samples were kept in a desiccator under nitrogen before the XPS measurements. All the CVs began and finished at 0.23 V. The fresh deposits showed already an extensive oxidation (Table III) .

The wide scan XPS spectra (not shown) of the cycled Pt-Ir/Ti deposits (451 scans for E_{pos}=0.86 V and 227 scans for E_{pos} = 1.1 V) show, besides the expected Ir and Pt signals, peaks corresponding to O, C, S, Cl and Ti. In agreement with previous SEM-EDAX work [20], the presence of Ti peaks suggests that the coverage of the Ti substrate by the Pt-Ir deposits is not uniform.

Figure 7 shows the Ir 4f and Pt 4f spectral regions. Due to their closeness, the fit of the Ir 4f and Pt 4f signals was done simultaneously. The number of spin-orbit doublets necessary to fit the spectra varied from sample to sample (Figure 7 and Table II). An additional peak appearing at ca. 62.3 62.5 eV and which corresponds to the Ti 3s level of the metallic substrate was also included in the fit (Figure 7). In order to obtain a satisfactory convergence and to avoid unrealistic results a series of constraints were used in the fitting procedure:

(i) the exponential tail of the peaks corresponding to the Pt° 4f doublet was kept fixed to the value obtained from the fit of the Pt 4f doublet recorded from a fresh Pt electrode.
(ii) the $4f_{5/2}/4f_{7/2}$ peak area ratio was fixed to the theoretical value of 0.75.
(iii) the linewidths of all the Pt contributions were fixed to be equal.
(iv) the linewidths of all the Ir contributions were fixed to be equal.
(v) the width of the Ti 3s peak was fixed during the first steps of the fitting procedure to the value obtained from the fit of the Ti 3s peak recorded from a fresh Ti foil, and was left to refine during the last steps of fitting.

The contribution of Pt signals to the Ir 4f region due to the Al Ka_3 X-ray satellite was not taken into account, since these Pt signals are expected to appear at 9.8 eV below the main Pt peaks, and have an intensity of about 4% of the main peaks [30]. In the cases were the Pt 4f signal is intense and the Ir 4f signal weak, the relative intensities obtained for the Ir° signals must be, thus, taken with caution because they can be affected by a large uncertainty.

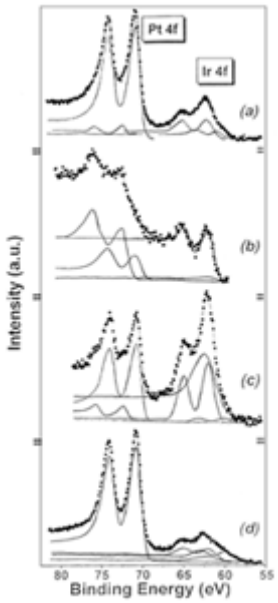

Fig.7. Enlarged signal between 80 and 55 eV for the XPS Pt 4f and Ir 4f spectra of Pt-Ir/Ti electrode cycled at 0.1 V s^{-1} in 0.5 M H_2SO_4 up A: After 227 cycles up to 1.1V in 0.5 M H_2SO_4 + 1 M CH_3OH. B: After 451 cycles up to 0.86 V in 0.5 M H_2SO_4 + 1 M CH_3OH. C: After 227 cycles up to 1.1 V in base electrolyte. D: After 451 cycles up to 0.86 V in base electrolyte.

Table II. Binding energies of cycled Pt-Ir/Ti electrodes obtained by fitting of the spectra shown in Figure 8.

Cycling conditions	Pt $4f_{7/2}$(eV)	Δ_{Pt}(eV)	Ir $4f_{7/2}$(eV)	Δ_{Ir}(eV)	Ti3s(eV)	Assignment
E_{pos}=	70.8	3.3				Pt^0
0.86 V	72.5	3.3				P^{2+}
no			60.6	2.9		Ir^0
methanol			62.2	2.9		Ir^{4+}
					62.4	Ti^{4+}
E_{pos}=	70.8	3.3				Pt^0
0.86 V	72.6	3.3				Pt^{2+}
			62.1	2.9		Ir^{4+}
methanol					62.3	Ti^{4+}

E_{pos}=	70.7	3.3				Pt^0
1.10 V	72.4	3.3				Pt^{2+}
no			60.2	2.9		Ir^0
methanol			62.0	2.9		Ir^{4+}
					62.5	Ti^{4+}
E_{pos}=	70.7	3.3				Pt^0
1.10 V			60.1	2.9		Ir^0
			62.1	2.9		Ir^{4+}
methanol					62.3	Ti^{4+}

Δ_{Pt} and Δ_{Ir} are the splitting between the Pt $4f_{7/2}$and Pt 4f5/2 and Pt $4f_{5/2}$and the Ir $4f_{7/2}$and Ir $4f_{5/2}$peaks, respectively.

The results presented in Figure 7 and Tables II and III indicate that the surface of the fresh Pt-Ir/Ti deposits had an Ir:Pt ratio of 0.8, which is about twice higher than that in the bath, 0.43. Both Pt and Ir were extensively oxidized, especially Ir, in which 88% of the atoms were present as Ir^{4+}.

Table III. Atomic ratios obtained from the fit of the XPS spectra shown in Figure 8.

Epos/Volts	methanol	*Ir(total)* / *Pt(total)*	*Pt* $^{2+}$ / *Pt*	*Ir* $^{4+}$ / *Ir*
0.86	no	0.34	0.10	1.77
	yes	0.48	1.96	
1.1	no	1.03	0.18	11.0
	yes	0.32	0.00	1.18
Fresh electrode		0.8	0.3	7.3

Effect of cycling up to 0.86 V.

Both in the absence and presence of methanol, cycling up to 0.86 V decreased the Ir_{total}/Pt_{total} ratio of Pt-Ir/Ti deposits to about half the value for the fresh deposit. The simplest explanation of this decrease would be a dissolution of Ir, but this is very improbable, since the 20% decrease in total mass change (Fig. 5 C) is in good agreement with the 25% decrease in R_F. Furthermore, no mass decreases were observed when the potential was held for 100 s at 1.1 V, at which the dissolution rate would be highest.

After cycling up to 0.86 V in the absence of methanol the Pt^{2+}/Pt^0 ratio decreased to one third of its value for the fresh electrode, which points to a reduction of the native Pt(II) oxide. However, after cycling in the presence of methanol the Pt^{2+}/Pt^0 ratio was 6.5 times higher than that for the fresh electrode, indicating that the Pt oxide formed in the presence of methanol is more difficult to reduce than that formed in its absence.

The effect of cycling up to 0.86 V on the Ir^{4+}/Ir^0 ratio was similar to that on the Pt^{2+}/Pt^0 ratio: cycling in the absence of methanol decreased it to one fourth of its value for the fresh electrode, while cycling in the presence of methanol increased it to infinity, *i.e.* all the surface Ir became Ir^{4+}. Similarly to the case of Pt, it is clear that the Ir(IV) oxide formed in the presence of methanol is more difficult to reduce than that formed in its absence. It should be emphasized that these measurements were carried out in duplicate.

Effect of cycling up to 1.1 V.

Cycling 200 times up 1.1 V in 0.5 M H_2SO_4 produced an enrichment in total Ir of about 30%, which cannot be explained by the growth of an Ir oxide layer, since the total mass change decrease of 35% is clearly due to an R_F decrease of 29% (Fig. 5 D). Therefore, this Ir enrichment should rather be due to a preferential migration of Ir atoms towards the surface during the sintering process. On the contrary, cycling up to 1.1 V in the presence of methanol decreased the Ir_{total}/Pt_{total} ratio by 60%, as if methanol assisted the dissolution of the Ir oxides. Actually after 200 cycles with methanol the total mass change decreased by 15% (Fig. 7 B), but again this decrease is due to sinterization, since R_F decreased by 28%.

Cycling up to 1.1 V in the absence of methanol decreased the Pt^{2+}/Pt^0 ratio to two thirds of its value for the fresh electrolyte, pointing to a reduction of the native Pt(II) oxides, as already observed when cycling up to 0.86 V. This reduction was even stronger when cycling in the presence of methanol, after which no Pt(II) oxides remained on the surface of the deposit. This result is completely opposite to that obtained when cycling up to 0.86 V, when the Pt^{2+}/Pt^0 ratio increased to a value 6.5 times higher than that for a fresh electrode. Apparently the reducibility of the Pt(II) oxide formed in the presence of methanol is most sensitive to the upper potential limit used in cycling.

Cycling up to 1.1 V in the absence of methanol increased the Ir^{4+}/Ir^0 ratio by 50%, due to an increased growth of Ir(IV) oxide. Methanol increased the reducibility of the Ir(IV) oxide, since cycling in the presence of methanol decreased the Ir^{4+}/Ir^0 ratio to 16% of its value for a fresh electrode. If the electrooxidation of methanol occurs by chemical reaction with Ir(IV) oxide, followed by immediate reoxidation of the latter and further repetition of the process, it could be envisaged that the Ir(IV) oxide subjected to this

process of continuous formation and reduction would be more completely reducible than that formed in the absence of methanol.

It should be stressed that no conclusions on the reducibility of Pt or Ir oxides can be obtained from CVs recorded in the presence of methanol, since most of the current corresponds to the electrooxidation of methanol, to the point that no cathodic current of metal oxide reduction appears in the negative sweep (Fig. 6 A). However, the mass response can throw light on this issue, since oxide formation and reduction produce large mass changes. So, it can be clearly appreciated that in the first CV (solid line in Fig. 6 B) the mass decrease corresponding to reduction of the metal oxide is very steep, which indicates a prompt reduction of the oxide. The mass decrease becomes markedly less steep with cycling (dashed and dotted lines in Fig. 6 B), pointing to a more difficult reducibility of the oxide, but this cannot be appreciated at all in the CVs, in which the ascending branch of the anodic peak in the negative sweep, in the potential region over which oxide reduction takes place, is practically the same in the 1^{st}, 5^{th} and 200^{th} CV (Fig. 6 A). The XPS results apparently contradict this EQCM result, that cycling in methanol decreases the reversibility of the oxide reduction on Pt-Ir, since cycling in the presence of methanol decreased the $Ir^{4+}/Ir°$ ratio to 16% of its value for a fresh electrode. However, it is possible that with methanol the reduction of the oxide, although more difficult, would be more complete.

CONCLUSIONS

The activity of 70:30 Pt-Ir wires and electrodeposits for methanol electrooxidation was similar to that of pure Pt, since in both Pt-Ir alloys electrooxidation of the metal started at about the same potential as on Pt.

Cycling of Pt-Ir deposits produced a decrease of roughness, but without a proportional decrease of the activity for methanol electrooxidation. The total mass change between the negative and positive potential limits of the scan decreased with potential cycling, and this decrease was approximately proportional to the decrease of the roughness factor, as was to be expected.

According to *ex situ* XPS analyses cycling in the absence of methanol decreased the Ir/Pt ratio to one half of its value for the fresh deposit if the upper potential limit was 0.86 V *vs.* SCE, but increased it by 30% if the said limit was increased to 1.1 V, which should be due to the growth of an Ir oxide layer. After cycling up to 1.1 V in the presence of methanol no Pt(II) species remained on the surface, and the fraction of Ir(IV) species decreased very much. This increase of the reducibility of the metal oxides was attributed to their acting as intermediaries in the electrooxidation of methanol.

* Corresponding author

ACKNOWLEDGMENTS

The authors are grateful to the DICYT-USACH and FONDECYT for grant 2970020. C.Y. is grateful to CONICYT-CHILE for a doctoral fellowship.

REFERENCES

1. T.D. Jarvi, E.M. Stuve, in *Electrocatalysis* (Edited by J. Lipkowski and P.N. Ross) Chap. 3, p.75. Wiley-VCH, Inc. (1998).

2. S. Wasmus, A. Küver, J. Electroanal. Chem., **461,** 14 (1999).

3. R. Parsons and T. van der Noot, J. Electroanal. Chem. **257,** 9 (1988).

4. H. A. Gasteiger, N. Markovic, P. N. Ross Jr. and E. J. Cairns, Electrochim. Acta **39,** 1825 (1994).

5. X. H. Xia, T. Iwasita, F. Ge and W. Vielstich, Electrochim. Acta **41**, 711 (1996).

6. M. Beltowska-Brzezinska and T. Luczak, J. Appl. Electrochem. **27**, 999 (1997).

7. J. Munk, P. A. Christensen, A. Hamnett and E. Skou, J. Electroanal. Chem. **401,** 215 (1996).

8. B. Beden, A. Bewick, K. Kunimatsu and C. Lamy, J. Electroanal. Chem. **121**, 343 (1981).

9. D. A. Buttry in *Electrochemical Interfaces: Modern Techniques for In-Situ Interface Characterization*. (Edited by H.D. Abruña) chap.10, p.531. VCH-publishers, (1991).

10. M. Hepel, Electrochim. Acta **41**, 63 (1996).

11. J. Willsau, O. Wolter and J. Heitbaum, J. Electroanal. Chem. **194**, 27 (1985).

12. M. S.Ureta-Zañartu, P. Bravo and J. H. Zagal, J. Electroanal. Chem. **337**, 241 (1992).

13. R. Ortiz, O. P. Márquez, J.Márquez and C.Gutiérrez, J. Phys.Chem. **100**, 8389 (1996).

14. M. M. Hefny and S. Abdel-Wanees, Electrochim. Acta **41,** 1422 (1996).

15. L. D. Burke and D. T. Buckley, J. Electrochem. Soc. **143**, 845 (1996).

16. N. M. Markovic, H. A. Gasteiger, P. N. Ross Jr., X. Jiang, I. Villegas and M. J. Weaver, Electrochim. Acta **40**, 91 (1995).

17. M. Krausa and W. Vielstich, J. Electroanal. Chem. **379**, 307 (1994).

18. P.C. Biswas, Y. Nodasaka, M. Enyo and M. Haruta, J. Electroanal. Chem. **381,** 167 (1995).

19. D. Chou and S. Gilman, J. Electrochem. Soc. **143**, 1685 (1996).

20. S. Ureta-Zañartu, C. Yáñez, G. Reyes, J. R. Gancedo and J. F.Marco, J. Solid. State Electrochem. **2**, 181 (1998).

21. M. S. Ureta-Zañartu, C. Yáñez, M. Páez and G. Reyes, J. Electroanal. Chem. **405**, 159 (1996).

22. C. D. Wagner, L. E. Davis, M. V. Zeller, J. A. Taylor, R. M. Raymond and L. H. Gale, Surf. Interf. Anal. **2**, 222 (1980).

23. J.O. Zerbino, N.R. de Tacconi and A.J. Arvía, J. Electrochem. Soc., **125**, 1226 (1978).

24. J. A. Caram and C. Gutiérrez, J. Electroanal. Chem. **323**, 213 (1992).

25. A. Aramata, T. Yamazaki, K. Kunimatsu and M. Enyo, J. Phys. Chem. **91,** 2309 (1987).

26. W. Visscher, J. F. E. Gootzen, A. P. Cox and J. A. R. van Veen, Electrochim. Acta **43**, 533 (1998).

27. C. P. Wilde and M. Zhang, Electrochim. Acta **39**, 347 (1994).

28. F. Gloaguen, J.M. Léger, C. Lamy, J. Electroanal. Chem., **467**, 186 (1999)

29. T. Frelink, W. Vissher, J.A.R. van Veen, Langmuir **12**, 3702 (1996)

30. *Handbook of X-Ray Photoelectron Spectroscopy* (Edited by C. D. Wagner, W. M. Riggs, L .E. Davis, J. F. Moulder and G. E. Muilenberg), p. 13.Perkin-Elmer Corp., Physical Electronics Divission, Eden Prairie, Minnesota (1978),